PHYSICAL REVIEW B **88**, 014521 (2013)

Phases of superfluid helium in smooth cylindrical pores

Timothy R. Prisk,[1] Narayan C. Das,[1] Souleymane O. Diallo,[2] Georg Ehlers,[2] Andrey A. Podlesnyak,[2] Nobuo Wada,[3]
Shinji Inagaki,[4] and Paul E. Sokol[1]
[1]*Department of Physics, Indiana University, Bloomington, Indiana 47408, USA*
[2]*Quantum Condensed Matter Division, Oak Ridge National Laboratory, Oak Ridge, Tennessee 37381, USA*
[3]*Department of Physics, Nagoya University, Chikusa-ku, Nagoya 464-8602, Japan*
[4]*Toyota Central R&D Laboratories, Inc., Yokomichi, Nagakute, Aichi 480-1192, Japan*
(Received 6 September 2012; revised manuscript received 25 May 2013; published 23 July 2013)

This paper reports an inelastic neutron scattering study of superfluid helium confined with highly monodisperse, smooth, and unidimensional silica pores only a few nanometers in diameter, previously studied only by means of macroscopic, thermodynamic techniques. Helium gas sorption isotherms show that the adsorption of helium gas proceeds by film growth, providing quantitative information about the thickness of the adsorbed film and its two-dimensional compressibility. Two different microscopic phases were observed using inelastic neutron scattering. When the adsorbed superfluid helium forms a thin film only a few atomic layers thick, it supports a dramatically modified phonon-roton spectrum as well as a compressed layer roton. The energies of these modified phonon-roton modes are consistent with those of a dilute, low-density film, one in which the average interatomic spacing is greater than in the bulk liquid. In contrast, when the pores are saturated with liquid, the modified phonon-roton spectrum disappears, and instead bulklike modes coexist with the compressed layer mode. The qualitative difference between these two pore-filling regimes is reflected in the effective vibrational density of states.

DOI: 10.1103/PhysRevB.88.014521 PACS number(s): 67.25.dt, 03.65.Vf, 78.70.Nx

I. INTRODUCTION

Liquid helium within restricted geometries has proved to be a fruitful playground for exploring the effects of confinement, quenched disorder, and reduced dimensionality on quantum liquids.[1] Interesting and nontrivial changes occur to the physical properties of liquid ^{4}He in confinement, including changes in critical exponents, thermodynamic functions, and transport properties.[2] On flat surfaces, thin films of liquid helium undergo the two-dimensional (2D) Kosterlitz-Thouless phase transition.[3,4] Within porous media, a finite-sized generalization of the Kosterlitz-Thouless transition occurs because of the restricted geometry.[5–7] Furthermore, when pores are saturated with liquid helium, the properties of the confined fluid remain altered in a number of important respects. The superfluid phase transition temperature T_S is suppressed from the bulk λ-point temperature T_λ. Confinement within mesoporous media also modifies the way in which the heat capacity C and superfluid fraction ρ_s depend upon temperature.

In order to study the microscopic dynamics underlying these changes, inelastic neutron scattering has been extensively used to probe the elementary excitations of liquid helium adsorbed to planar surfaces like graphite[8,9] and within a variety of porous glasses, such as aerogel,[10–13] Vycor,[14,15] xerogel,[16] Geltech,[17] Mobil Crystalline Material (MCM)-41,[18] and MCM-48.[19] A “global picture” of the excitations of the restricted liquid has emerged from these studies.[1] Two distinct branches of collective excitations are observed when the pores are full of superfluid helium. The first is a bulklike phonon-roton spectrum representing liquid within the core volume of the pores. These modes have energies which closely coincide with those of the true bulk liquid. The second is a layer mode, or 2D surface roton, which exists within the high-density liquid layers close to the liquid-solid interface. These surface rotons are typically observed only around the first peak in the static structure factor $S(Q)$. In the neutron scattering data, they appear as additional intensity on the low energy side of the bulklike roton signal.

The thermodynamic behavior of the bulk superfluid ^{4}He, the heat capacity C, and superfluid fraction ρ_s in particular, can be explained by treating liquid helium as a weakly interacting gas of three-dimensional (3D) phonons and rotons.[20] Dimeo *et al.*[14] demonstrated that the existence of the layer mode in Vycor is responsible for the modified thermodynamic behavior of the confined liquid. They assumed that these new modes have a 2D density of levels and a rotonlike dispersion $E(Q) = \Delta + \hbar^2(Q - Q_R)^2/2\mu$, obtaining the Landau parameters by a fit to their neutron scattering data. Taking into account both 2D and 3D rotons, they reproduced the heat capacity C and superfluid fraction ρ_s measured by thermodynamic techniques.

Advances in the synthesis of mesoporous materials have produced materials with well-defined pores and smooth walls such as folded sheet material (FSM)-16, whose pores are monodisperse, only a few nanometers in diameter, and ordered in a regular triangular lattice structure.[21] Nuclear magnetic resonance (NMR) spectroscopy studies of the mobility of ^{3}He adsorbed within porous glasses have provided quantitative information about the atomic-scale roughness of these materials.[22–24] In Vycor, a spongelike borosilicate glass with a disordered pore network and rough internal surfaces, the atomic-scale irregularities of the substrate increase the effective strength of the adsorption potential, thereby hindering the lateral movement of adsorbed atoms.[25] Within the quantum tunneling regime, the relaxation time of ^{3}He atoms is shorter within FSM-16 than Vycor by an order of magnitude. Within MCM-41, a template silica glass structurally very similar to FSM-16, the relaxation time is longer by roughly a factor of two. This indicates that the probability amplitude for ^{3}He to tunnel form one adsorption site to another is comparatively large, implying smooth pore walls with relatively small tunneling barriers between adsorption sites. The pore walls of MCM-41 are generally considered rough and heterogeneous.[26]

Wada *et al.* have performed torsional oscillator and heat capacity measurements of liquid helium films adsorbed within FSM-16 as a function of temperature, pore filling, and channel diameter, finding good evidence that adsorbed thin films show 2D behavior.[27,28] Their measurements suggest that thin films of ^{4}He in 28 Å FSM-16 pores undergo a finite-sized Kosterlitz-Thouless phase transition in which vortex-antivortex pairing is influenced by strong confinement forces stemming from the restricted geometry.[7] The heat capacity at very low temperatures T varies as T^2, as expected from a phonon gas in reduced dimensions.[29,30] Furthermore, the inferred velocity of first sound in the adsorbed films is depressed below the speed in the bulk liquid. Therefore, one expects that the inherently 2D nature of the film is reflected in its collective excitation spectrum.

In this paper, we report inelastic neutron scattering measurements of the collective excitation spectrum of liquid ^{4}He adsorbed within 28 Å FSM-16 pores. The new results sweep across the phase diagram previously determined by torsional oscillator studies, providing information about the excitations as a function of temperature and pore filling. In very thin films, we observe a dramatically modified phonon-roton spectrum coexisting with the surface roton. The energies of these modes are consistent with variational predictions for a dilute film,[31,32] confirming predictions that, in smooth and well-defined pores, one may observe a dilute, low-density film.[33] At the same time, the energy of the surface roton is consistent with that of a dense liquid, indicating that the adsorbed thin film does not have a single, uniform density. This suggests a previously unknown relationship between atomic-scale roughness of the substrate and the surface rotons: surface roughness locally increases the effective surface adsorption potential, thereby compressing small regions of the adsorbed film and permitting only short-wavelength, rotonlike excitations in these regions. Upon filling of the pores, the surface roton strengthens in intensity, and a bulklike phonon-roton spectrum coexists with the surface roton. Presumably, at full pore, bulklike liquid occupies the core volume of the pores and compresses the surface layers near the interface with the solid. These changes in the spectrum clearly connect the character of the excitations to the local density of the liquid.

II. THEORETICAL BACKGROUND

The phonon-roton spectrum of the bulk liquid is closely connected to the density of the liquid.[34] Under positive pressure, the phonon velocity is increased, and the maxon energy is enhanced relative to its values at saturated vapor pressure. The properties of the roton also undergo significant changes: under the application of positive pressure, or increased density, the position of the roton minimum Q_R shifts to higher Q, the effective mass μ decreases, and the roton energy gap Δ contracts. First-principles Monte Carlo calculations of $S(Q,E)$ under negative absolute pressure, or reduced density, predict the opposite behavior in the phonon-roton spectrum.[35,36] The underlying connection between the excitation energies and the density of the bulk liquid was first shown theoretically by Feynman's single-mode approximation,[20] according to which the phonon-roton dispersion is given by $E(Q) = \hbar^2 Q^2/2mS(Q)$, where $S(Q)$ is the static structure factor. The first peak in $S(Q)$, given by $2\pi/b$, where b is the typical interatomic spacing, produces a roton minimum at roughly $Q_R \sim 2\pi/b$. More sophisticated variational calculations of the phonon-roton spectrum which account for "backflow"—the coupling of the bare excitations to a cloud of virtual phonons and rotons—share a systematic relationship between the properties of the roton and the density of the superfluid.[37,38] These theories predict that lowering the interparticle spacing increases the phonon velocity, decreases the roton energy gap, and shifts the roton minimum Q_R to higher Q, corresponding to a shift in the first peak in $S(Q)$ to higher Q.

The excitation spectrum of 2D planar helium[39,40] has been calculated at a series of areal densities by the variational method using both correlated basis functions[31] and shadow wave functions.[32] Within the liquid region of the phase diagram, the interparticle spacing of the film is greater than the bulk liquid, suggesting that it is a more weakly bound condensed phase. Both trial wave functions predict a shift in the roton minimum Q_R with the shift in the first peak in $S(Q)$.

Across the range of pore sizes and geometries, the presence of a layer mode emerges as a globally unifying feature of nanoconfined superfluid helium. The dispersion of these layer modes, however, depends upon the confining matrix. Apaja and Krotscheck[33] have argued that the layer modes are predominately shaped by the local adsorption potential of the porous host, rather than by its more global, morphological features. In particular, the energy gap of the layer modes sensitively depends upon the adsorption potential in the liquid layers they inhabit.

Apaja and Krotscheck also calculated the spectrum for thin films, which are not strictly 2D. They predicted that thin films adsorbed in porous media have a low overall "effective" density due to the energy costs of forming a free surface. Therefore, the energies of the phonon-roton modes should in some sense correspond to the microscopic properties of the bulk liquid under negative pressure. In order to verify this prediction, they recommended experimental investigation of porous materials with a uniform distribution of small pores. The results of such an investigation are reported in this paper.

Ab initio calculations predict that liquid helium confined within nanometer-scale cylindrical pores form concentric atomic layers with about 3 Å spacing.[41] There have been quantum Monte Carlo simulations[42] of thin helium films on planar silica with a potential well depth of ~100 K. This is close to the differential binding energy of helium atoms to the FSM-16 substrate,[43] which is the low coverage heat of adsorption $q_{st} \sim 110$ K. According to these calculations, the first adsorbed layer forms an inert solid in which the atoms are highly localized and spatially segregated from higher layers. There are atomic exchanges within the second layer, and exchanges both within and between higher layers. It is likely that a similar picture also applies to liquid ^{4}He confined with FSM-16 with modifications due to the tight curvature of the pore walls.

III. EXPERIMENTAL APPROACH

A. Sample characterization

We synthesized the powdered FSM-16 using methods described in detail elsewhere.[21] A silicate-organic complex is produced from kanemite paste ($Na_2Si_2O_5$) and alkyltrimethylammonium [$C_nH_{2n+1}N^+(CH_3)_3$] bromide/chloride and heated. At the first stage of the synthesis process, parallel and regularly waved silicate sheets penetrate through aggregations of surfactants to which they are ionically bonded. Due to the aggregation of surfactant ions, interlayer crosslinking bends the silicon-oxygen bonds of the sheets, folding them into a regular pore structure. The surfactants in the resulting silicate-organic complex are removed by calcination, leaving behind an ordered mesoporous molecular sieve, FSM-16.

The sample material was characterized using a combination of small-angle x-ray scattering[44,45] and gas sorption isotherms.[46,47] Together these measurements establish the phase purity of the sample, the crystallinity of its pore array, monodispersity, geometry, and size of its pores.

X-ray scattering measurements were performed using Cu Kα radiation from a rotating anode source. The ordered pore array of FSM-16 forms a 2D triangular lattice (plane space symmetry group $p6mm$) with center-to-center spacing a. The x-ray scattering data therefore shows a series of small-angle diffraction peaks located at wave vector transfers $Q_{(hk)} = (4\pi/a\sqrt{3})\sqrt{h^2+k^2+hk}$, where h and k are the Miller indices of the peaks. As shown in Fig. 1, there are four clearly discernible (hk) Bragg reflections located at $Q_{(10)} = 0.16$ Å^{-1}, $Q_{(11)} = 0.27$ Å^{-1}, $Q_{(20)} = 0.32$ Å^{-1}, and $Q_{(21)} = 0.42$ Å^{-1}. This corresponds to lattice constant of $a \approx 45$ Å.

In order to verify the pore geometry and obtain estimates of the pore size distribution $P(d)$, specific surface area S, and specific pore volume V, we measured an N_2 adsorption isotherm at 77 K on the FSM-16 sample used in the neutron scattering measurements. The FSM-16 sample was enclosed within a sealed cell, outgassed, and then submerged in an open dewar of liquid N_2. Conventional volumetric techniques were used to control the amount of gas loaded to the sample and obtain the vapor pressure of the adsorbed N_2 as a function of filling.

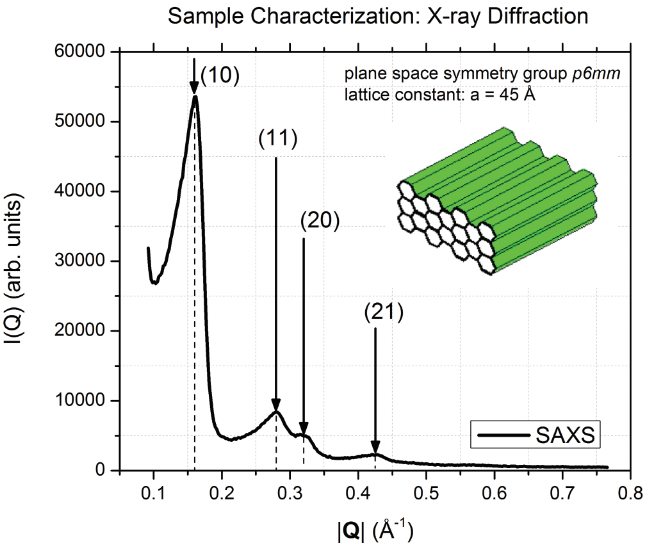

FIG. 1. (Color online) The ordered pores of FSM-16 comprise a 2D triangular lattice structure, and four clearly discernible Bragg reflections are observed, corresponding to a center-to-center pore spacing of 45 Å.

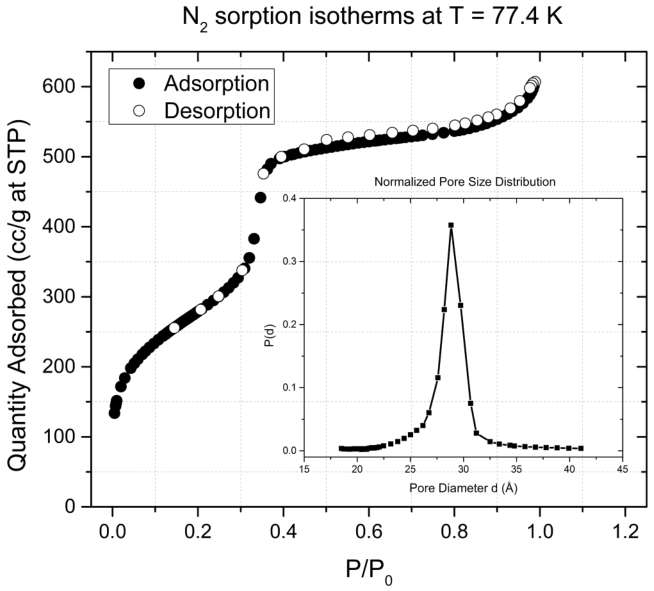

FIG. 2. The N_2 adsorption isotherm is Type IV and has a steep capillary condensation branch with no detectable hysteresis. The pore size distribution, calculated from the capillary condensation branch, is sharply peaked near 28 Å and has a full width at half maximum of ~2 Å. The specific internal surface area of the sample, determined by a BET plot for pressures $0.05 < P/P_0 < 0.2$, is 1015 m^2/g.

Figure 2 shows that the isotherm is Type IV according to the 1985 International Union of Pure and Applied Chemistry (IUPAC) classification.[48] The specific surface area S determined by a Brunauer-Emmett-Teller (BET) plot[49] for pressures $0.05 < P/P_0 < 0.2$ is 1015 m^2/g. The N_2 adsorption isotherm has a steep capillary condensation branch with no detectable hysteresis. The pore size distribution $P(d)$, calculated from the capillary condensation branch using both the Pierce[47] and Barrett-Joyner-Halenda[50] methods, is sharply peaked near 28 Å and has a full width at half-maximum (FWHM) of ~2 Å. The pore walls, therefore, have a thickness of 17 Å.

The state of helium confined in FSM-16 has been previously characterized by helium gas sorption isotherms at a series of different temperatures.[43] The isotherm data shows that the adsorption of ^{4}He proceeds by multilayer film growth with no capillary condensation. It can also be used to calculate the thickness δ of the adsorbed film, its 2D isothermal compressibility κ_T, and heat of adsorption q.

We measured the ^{4}He adsorption isotherm at 4.2 K on the FSM-16 sample used in this study using the same open dewar setup as the N_2 adsorption measurements and the sample cell used in the neutron scattering measurements. The shape of the isotherm, shown in Fig. 3, confirms that ^{4}He adsorption proceeds by multilayer film growth and is in good agreement with previous results. A BET analysis of $0.05 < P/P_0 < 0.35$ gives monolayer coverage at $n_1 = 21.9$ mmol/g, or at an areal density of 21.6 μmol/m^2. For comparison,[18] monolayer coverage on graphite takes place at 19.1 μmol/m^2 and on the pore walls of MCM-41 at about 25.7 μmol/m^2. It is likely that this first layer is an amorphous solid.[18,42,51] Saturated vapor pressure is achieved at roughly $n_{\mathrm{svp}} = 47$ mmol/g. Assuming that the solid layer is 4 Å thick, full pore filling can be estimated to occur around 45 mmol/g gas loading if

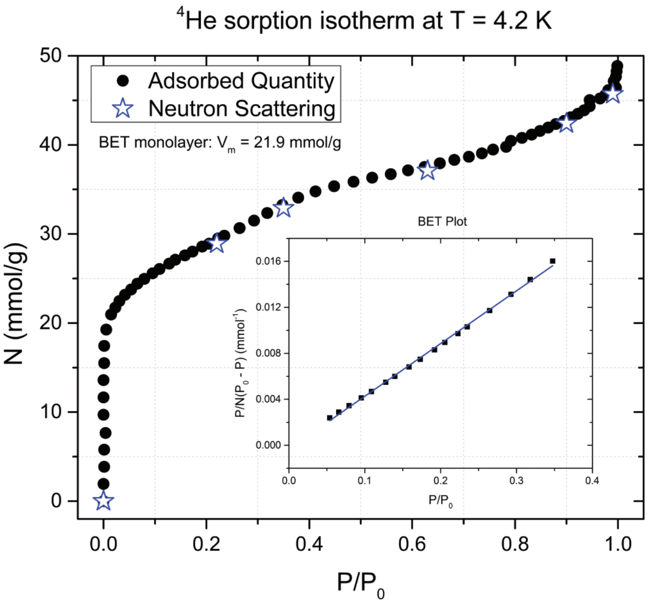

FIG. 3. (Color online) ^{4}He adsorption isotherm at 4.2 K taken on the sample used in the neutron scattering study. The shape of the isotherm suggests multilayer film growth, while the inset BET plot shows that monolayer completion takes at 21.9 mmol/g. Saturated vapor pressure is achieved roughly at $n_{\text{svp}} \sim 47$ mmol/g. The stars denote fillings where neutron scattering measurements were performed.

the remaining liquid is at bulk density. Therefore, at full pore, the adsorption isotherm is consistent with the presence of some liquid beyond the monolayer having higher density than bulk.

Gas sorption isotherms contain quantitative information about the thickness δ of the adsorbed film, its 2D isothermal compressibility κ_T, and the isoteric heat of adsorption q_{st}.[43,46,52] According to the Frenkel-Halsey-Hill model, the chemical potential μ of the adsorbed atoms is reduced from the chemical potential of the bulk liquid by an amount equal to the binding energy of the substrate potential $-\Lambda/\delta^3$, where Λ is a constant. The equilibrium vapor pressure, which is related to the chemical potential μ, can therefore be used to calculate the thickness of the adsorbed film at a given gas loading. Notice that this model is strictly applicable only to thick films on planar substrates, where the van der Waals potential of the surface varies as the inverse cube of the distance from the surface. Nevertheless, this model provides reasonable empirical information for atomic and intermediate thickness films and forms the basis for more sophisticated models of thin helium films.[52–54] Figure 4 shows the estimated film thickness δ as a function of pore filling n based on the Frenkel-Halsey-Hill model. The helium film increases linearly in statistical thickness until $n_f = 36.3$ mmol/g, where there is a distinct change in the slope. The 2D isothermal compressibility $\kappa_T = -1/A(\partial A/\partial P)_T$ can be calculated from the adsorption isotherm data using the expression $(S/n^2RT)(\partial \ln P/\partial n)_T{}^{-1}$. Figure 4 also plots κ_T versus n. Coinciding with the change in slope of δ versus n, there is a local minimum in the compressibility κ_T at n_f, clearly signaling structural changes in the adsorbed film. The filling n_f probably corresponds to the complete formation of a fluid second layer given the estimated film thickness at this filling is approximately 7 Å, and there is a local minimum in κ_T at n_f, as observed upon layer completion in graphite.[42]

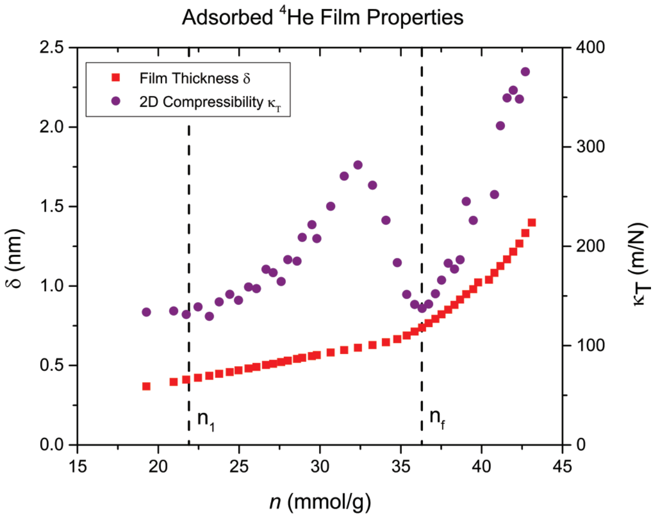

FIG. 4. (Color online) The adsorbed film thickness δ as a function of gas loading was calculated from the ^{4}He adsorption isotherm using the Frenkel-Halsey-Hill model. The thickness δ grows linearly with increasing pore filling until n_f, where there is a sudden change of slope. The purple circles denote the 2D isothermal compressibility κ_T of the adsorbed film. The filling $n_1 = 21.9$ mmol/g is to the inert solid layer, and $n_f = 36.3$ mmol/g likely corresponds to the complete formation of a fluid second layer.

B. Inelastic neutron scattering

Inelastic neutron scattering measurements of liquid helium confined in FSM-16 were carried out using the Cold Neutron Chopper Spectrometer (CNCS) at the Spallation Neutron Source.[55] The CNCS is a direct geometry time-of-flight spectrometer that receives a beam from a cold coupled moderator. The speeds and slit widths of the choppers can be varied, allowing adjustments in the instrumental resolution and intensity of the incident beam. An incident neutron energy of 3.65 meV ($\lambda = 4.73$ Å), which is below the Bragg edge of aluminum, was used to obtain a clean background signal with no strong spurious features. An oscillating radial collimator was used to reduce background scattering from the tail of the cryostat.

Our chosen chopper settings yielded an energy resolution at the elastic line of 81 μeV. Time-of-flight monitor data showed that the pulse width was 103 μs at the Fermi chopper and 27.6 μs at the double-disk choppers. We calculated the inelastic energy resolution from these pulse widths according to the Gaussian approximation. This calculation correctly reproduced the observed width of the elastic line. Near the bulk roton minimum $\Delta = 0.74$ meV, the neutron spectrometer's energy resolution is approximately 56 μeV. The measurements at 43.0 mmol/g gas loading were performed with different chopper settings, however, yielding a coarser energy resolution at the roton minimum of 63 μeV. The effective resolution function $R(\mathbf{Q},E)$ is very nearly Gaussian in energy E since neutrons are primarily selected by the choppers from the peak in the cold moderator's Maxwellian spectrum.

The sample cell is a cylindrical aluminum can with height $H = 5.71$ cm, inner diameter $d_i = 2$ cm, and wall thickness of 0.4 mm, and it seals by compressing an indium o-ring. Neodymium magnets were mounted to the sample cell to suppress the superconducting transition of aluminum. It was loaded with a mass of 4.62 g of FSM-16 and was subsequently degassed by pumping to a pressure $P < 10^{-3}$ torr at 80 °C for 24 h. Gas loading was performed *in situ* from an external gas handling system. The sample thickness was chosen to allow for approximately 93% beam transmission in order to minimize the effects of multiple scattering. An Oxford VeriCold dilution refrigerator was used to achieve low temperatures. The temperature was measured by a ruthenium oxide resistor thermally anchored to the mixing chamber. The sample cell mounts onto a copper support rod below the mixing chamber and is inside an evacuated space enclosed by the aluminum tail of the dilution refrigerator.

The detector intensities $I(\theta,\,\varphi,\,t)$ are measured within a solid angle $\delta\Omega$ as a function of neutron time-of-flight t and are converted using routines standard at the Spallation Neutron Source into intensities $\mathrm{I}(\mathbf{Q},E)$ at wave vector transfer $\mathbf{Q}$ and energy transfer E. The detector efficiencies were normalized by using a vanadium standard. If b is the scattering length of the ^{4}He nucleus, the instrument measures the double differential cross section per helium atom

$$\frac{d^2\sigma}{d\Omega dE} = \frac{Nb^2}{\hbar}\frac{k_f}{k_i} S(\mathbf{Q},E)\,.$$

The dynamic structure factor $S(\mathbf{Q},E)$ contains information about the density fluctuation spectrum in a condensed matter system.[56] In a classical liquid, it is related to the van Hove pair correlation function $G(\mathbf{r},\,t)$, which, given a particle at (0, 0), is the relative probability that there is a particle at $(\mathbf{r},t)$. In a quantum liquid,[34,57] $S(\mathbf{Q},E)$ is the Fourier transform of the time-dependent density-density correlation function $\langle\rho(\mathbf{Q},t)\rho^\dagger(\mathbf{Q},0)\rangle$, where ρ is the number density operator.

The energies, lifetimes, and spectral weights of the collective modes in a condensed matter system can be extracted from the "one-phonon" peaks in $S(\mathbf{Q},E)$. Model fits to our neutron scattering data were performed with the DAVE software package[58] developed by the National Institute of Standards and Technology. As discussed further below, we use the damped harmonic oscillator model to describe the intrinsic line shape of the phonon-roton peak, while a Gaussian model proved to satisfactorily represent the line shape of the surface roton. The measured dynamic structure factor is a convolution of the instrumental resolution function $R(\mathbf{Q},E)$ with the "true" scattering function: $S_{\mathrm{exp}}(\mathbf{Q},E) = S(\mathbf{Q},E) \otimes R(\mathbf{Q},E)$. The calculated inelastic energy resolution was folded into the model fit functions and then compared to the scattering data by a least-squares fit. Because the FSM-16 host is a powder, we observe a powder averaged dynamic structure factor $S(Q,E)$.

In a coherently scattering system like liquid ^{4}He, the vibrational density of states $G(E)$ can be obtained from the measured dynamic structure factor $S(Q,E)$ within the framework of the incoherent approximation.[56] If $S(Q,E)$ is considered by means of an average over a suitably large range in Q, it is appropriate to neglect interference effects between atoms and assume the scattering can be described in terms of incoherent scattering from individual, vibrating atoms. According to the incoherent approximation, then, the (one-phonon) dynamic structure factor $S(Q,E)$ can be written in terms of the partial density of states $G(Q,E)$:

$$S(Q,E) = e^{-2W}\frac{\hbar^2 Q^2}{2m}\frac{G(Q,E)}{E}\left[1+n(E,T)\right].$$

The partial density of states $G(Q,E)$ can therefore be obtained from the observed scattering $S(Q,E)$ by suitable Q- and E-dependent rescaling of the data. The Bose occupation factor $n(E,T)$ is given by $(1-e^{-E/k_BT})^{-1}$. Here, W is the Debye-Waller factor $\langle(\mathbf{Q}\cdot\mathbf{u})^2\rangle/3$. The effective vibrational density of states $G(E)$ is obtained by averaging $G(Q,E)$ over a large range $(Q_1,\,Q_2)$ in wave vector transfer

$$G(E) = \frac{1}{Q_2-Q_1}\int_{Q_1}^{Q_2} G(Q,E)\,dQ.$$

This procedure for extracting the effective density of states function $G(E)$ directly from the neutron scattering data neglects the contribution of multiphonon processes to the dynamic structure factor $S(Q,E)$. In contrast to one-phonon scattering, multiphonon processes typically do not contribute sharp peaks to $G(E)$ but instead yield a continuous spectrum which grows with increasing energy transfers E. Removing the multiphonon contribution from a direct determination of the density of states $G(E)$ using experimental neutron scattering data requires introducing a model for the multiphonon contribution. In this paper, we do not attempt to correct the experimental $G(E)$ for multiphonon processes but instead argue that, in this case, their central contribution to $G(E)$ can be readily identified by inspection.

IV. RESULTS

A. Raw data

The observed scattering at wave vector transfer $Q = 1.95$ Å^{-1}, including background scattering from the tail of the cryostat, is shown as a function of gas loading in Fig. 5. As can be seen, a clean background with no strong spurious features

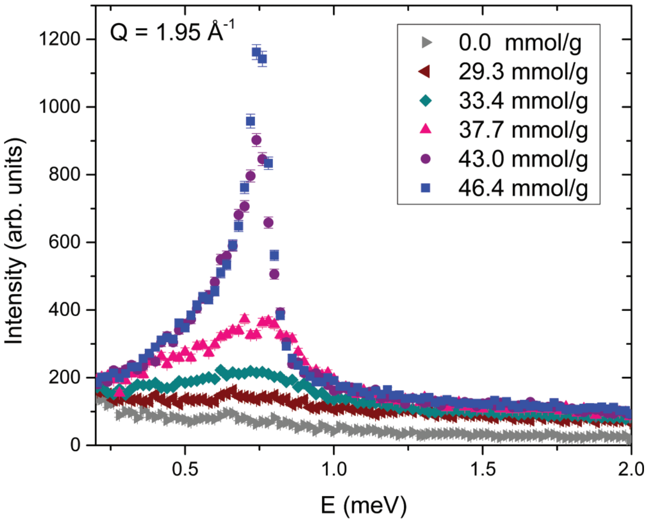

FIG. 5. (Color online) The dynamic structure factor at 49 mK (33 mK for the 43.0 mmol/g gas loading) without any background subtraction at wave vector $Q = 1.95$ Å^{-1}.

was obtained. For measurements taken at fillings 29.3 mmol/g gas loading (below $1.33n_1$) or at temperatures far within the normal liquid phase $T > T_S$, we observe only substratelike scattering and no well-defined excitations at any wave vector Q. The absence of sharply defined phonon-roton peaks at 29.3 mmol/g ^{4}He gas loading is consistent with the presence of an amorphous solid layer directly adsorbed to the pore walls. Superfluidity within porous media is usually observed in torsional oscillator measurements above about 1.4 atomic layers.[2,6,28]

As the filling is increased beyond the inert material, a distinct change in the scattering occurs. Phonon-roton excitations clearly emerge from the background scattering due to the porous host and the solid layer. In previous studies of liquid helium confined in porous glass, investigators observed "ghost" roton peaks, a Q-independent echo of the rotons associated with the multiple scattering of neutrons.[15–17] No such ghost roton peaks were present in our dataset. This is probably due to the fact that the sample cell was designed to allow for approximately 93% beam transmission at full pore, reducing multiple scattering to approximately 0.5% of the incident neutrons. Furthermore, the total amount of liquid ^{4}He within the cell is small, about 3.1 cm^3 at 46.4 mmol/g gas loading.

The dynamic structure factor of the adsorbed superfluid can be obtained by subtracting the contribution from the background, porous matrix, and the inert solid layer. Figure 6(a) shows the dynamic structure factor $S(Q,E)$ at 49 mK for 37.7 mmol/g gas loading, where the adsorbed helium forms a thin superfluid film on the pore walls. As can be seen, the scattering consists of a modified phonon-roton spectrum and has additional intensity below the roton minimum, implying the presence of a surface roton. For reasons discussed further below, we will refer to these as dilute layer modes (DLM) and compressed layer modes (CLM), respectively. For comparison, the bulk spectrum is shown as a dashed white curve.[59] It is clear from inspection that the phonon velocity is reduced, the maxon is softened, and the curvature of the roton region is altered relative to the bulk behavior. The observation of the long-wavelength phonon and intermediate-wavelength maxon suggests that the dilute layer modes involve the motion of atoms over an extended region in space. The dispersion of the excitations is insensitive to filling, to within our experimental uncertainties, in the range from 33.4 to 37.7 mmol/g, apart from the intensity and widths of the excitations.

At higher pore fillings, the nature of the excitations changes dramatically. Figure 6(b) plots $S(Q,E)$ at 46.4 mmol/g gas loading, where the pores are fully saturated with superfluid helium. The phonon-roton spectrum occurs at nearly bulk energies along with the additional intensity at low energy in the vicinity of the roton minimum. The excitation spectrum is insensitive to filling in the range from 43.0 to 46.4 mmol/g, aside from the strength and width of the excitations. A crossover from one regime to the other takes place around 40 mmol/g, although it is unknown how the spectrum evolves within this region. In both cases, no temperature dependence is observed below 1 K, and the well-defined modes altogether vanish as the temperature is raised far above the normal-superfluid transition temperature T_S determined by previous torsional oscillator measurements.[28]

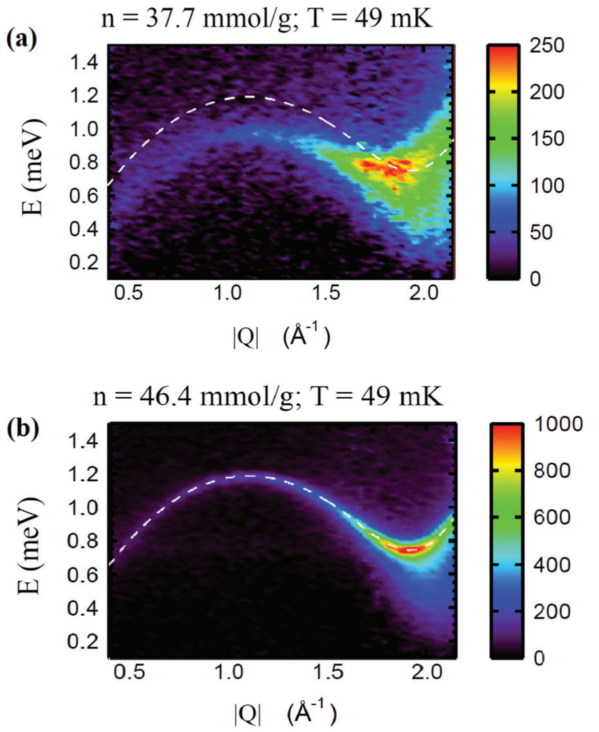

FIG. 6. (Color online) The dynamic structure factor $S(Q,E)$ at pore fillings 37.7 and 46.4 mmol/g at 49 mK, with the background subtracted. The dispersion of the bulk liquid is shown as a dashed white line. In the lower filling case, it is clear from inspection that the phonon velocity is reduced, the maxon is softened, and the curvature of the roton region is altered relative to the bulk behavior. In both filling regimes, additional intensity below the roton is observed, which indicates the presence of surface rotons within the system.

B. Density of states

The effective vibrational density of states $G(E)$ was calculated from the observed scattering $S(Q,E)$ using Eqs. (2) and (3). The effective mean-squared displacement $\langle u^2 \rangle$ can be estimated by assuming liquid helium has a Debye temperature Θ_D of 25 K.[34] At low temperatures, $\langle u^2 \rangle$ will be dominated by quantum-mechanical zero-point motion where $\langle u^2 \rangle = 9\hbar^2/4mk_B\Theta_D = 1$ Å^2. This is the approximately the value that the mean-squared displacement $\langle u^2 \rangle$ takes in hexagonal close-packed (hcp) solid helium,[60] suggesting that this is a reasonable estimate of the effective Deybe-Waller factor for the liquid. We integrated the partial density of states $G(Q,E)$ over wave vectors of 0.5 Å$^{-1} \leqslant Q \leqslant 1.9$ Å^{-1} to obtain $G(E)$. Finally, we carried out the same calculation using the known dispersion of the bulk liquid to obtain a theoretical effective density of states $G(E)$ for the bulk liquid.

Figure 7(a) plots the effective density of states $G(E)$ at 49 mK for three pore fillings when the background signal from the cryostat and empty matrix has been subtracted from the raw data. As can be seen, $G(E)$ at 29.3 mmol/g initially increases slowly and nearly monotonically. This reflects the absence of any well-defined excitations in $S(Q,E)$. This is again consistent with the presence of an amorphous solid layer on the pore walls. It is possible that the density of states of this inert helium in some sense mirrors that of the silica substrate. However, we are unable to confirm or disconfirm

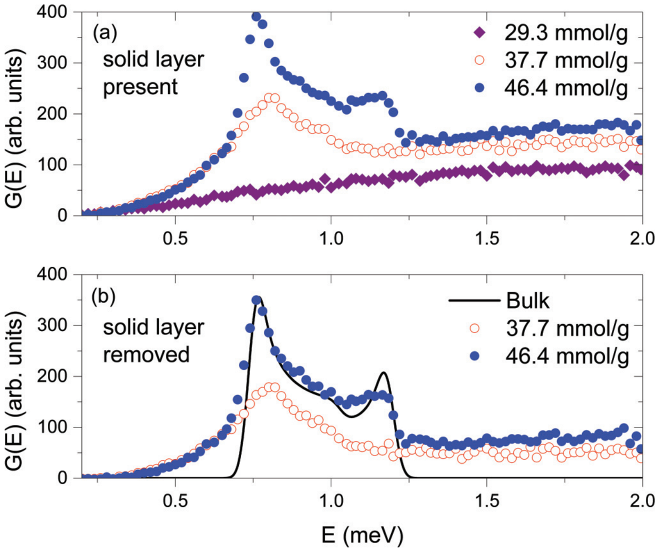

FIG. 7. (Color online) The effective density of states $G(E)$ for superfluid ^{4}He adsorbed in FSM-16 at 49 mK. The solid line is the calculated density of states of the bulk liquid.

this hypothesis since we did not perform neutron scattering measurements of the background without the presence of the empty FSM-16 substrate.

The effective vibrational density of states $G(E)$ of the bulk liquid is shown in Fig. 7(b). There are two peaks in $G(E)$, located at 0.75 and 1.20 meV, corresponding to the energies of the roton and maxon, respectively. If S is a surface of constant energy in reciprocal space, then the density of states $g(E)$ is related to the dispersion $E(\mathbf{k})$ by

$$g(E) = \int_S \frac{dS}{4\pi^3} \frac{1}{|\nabla_{\mathbf{k}} E(\mathbf{k})|}.$$

The two peaks occur because the gradient of the dispersion vanishes in the maxon and roton regions. This is directly analogous to van Hove singularities in solids, which occur whenever constant energy surfaces S in reciprocal space pass through points where $\nabla_{\mathbf{k}} E(\mathbf{k})$ vanishes. Beyond the maxon peak in $G(E)$, the one-phonon density of states drops to zero.

At 37.7 mmol/g, a thin fluid film supporting strongly modified phonon-roton excitations, as shown in Fig. 6(a), is present on top of the adsorbed solid layer. Figure 7(b) shows the calculated density of states when the inert layers are subtracted from the data. The CLM, which are not present in the bulk liquid, determine the form of $G(E)$ at energies below 0.65 meV. The dispersion of the DLM determines the shape of $G(E)$ between 0.65 meV $< E <$ 1 meV, forming an asymmetric peak with its maximum at 0.8 meV. Beyond the dilute layer maxon energy at 1 meV, $S(Q,E)$ recedes into what is presumably a broad multiphonon background. The density of levels $G(E)$ is finite beyond 1 meV because of this high-energy tail in $S(Q,E)$.

Figure 7(b) shows that the density of states is qualitatively changed at a gas loading of 46.4 mmol/g, when the pores are fully saturated with superfluid helium. At low energies $E <$ 0.65 meV, the compressed layer rotons continue to govern the density of levels, and $G(E)$ is unaltered from the thin film case. However, within the energy range 0.65 meV $< E <$ 1.25 meV, the density of levels is found to closely coincide with the calculated density of states of the bulk liquid. Again, beyond the maxon energy at 1.25 meV, multiphonon processes produce a tail in the calculated $G(E)$. Because the primary multiphonon contribution to the calculated $G(E)$ is already evident upon inspection, we have not attempted to introduce any models for multiphonon corrections.

C. Model line shapes

In order to determine the energies, inverse lifetimes, and spectral weights of the elementary excitations, we performed least squares fits of $S(Q,E)$ versus E, folding in the calculated resolution function $R(E)$ of the neutron spectrometer. The line shape of the bulk liquid excitations is modeled by the damped harmonic oscillator (DHO) peak,[56,57,61] which describes dynamic susceptibility of a harmonic oscillator to an external perturbation. We found that, for $Q \leqslant 1.70$ Å^{-1}, the data could be fit to the sum of a DHO peak and a linear background. This linear background presumably captures the contribution to $S(Q,E)$ from multiphonon processes. The DHO peak has the following form:

$$S_{\text{ext}}(Q,E) = \frac{n(E,T)}{2\pi} Z(Q) \left\{ \frac{\Gamma}{[E - E_m(Q)]^2 + (\Gamma/2)^2} - \frac{\Gamma}{[E - E_m(Q)]^2 + (\Gamma/2)^2} \right\}.$$

Where $Z(Q)$ is the oscillator strength, Γ is the FWHM, and E_m is the peak center, which are freely varying fit parameters. The Bose occupation factor $n(E,T) = (1 - e^{-E/k_BT})^{-1}$ accounts for the thermal population of the excitations at equilibrium temperature T.

Figure 8 compares, for 37.7 and 46.4 mmol/g gas loading, the resolution broadened fits to the experimental data within the maxon region $Q = 1.15$ Å^{-1}. The data clearly shows the dependence of the maxon energy with pore filling. The model fits the data well, where χ^2 is equal to 1.3 and 1.8, respectively. A calculation of the correlation matrix shows that the free parameters of the damped harmonic oscillator are not strongly correlated.

At larger wave vector transfers $Q \geqslant 1.75$ Å^{-1}, there is additional intensity due to the presence of CLM. Following the literature,[14–18] we fit this peak to a Gaussian:

$$S_{\text{CLM}}(Q,E) = \frac{A}{\sigma\sqrt{2\pi}} e^{-[E - E_L(Q)]^2/2\sigma^2},$$

where A is the area of the Gaussian, σ^2 is the second moment of the peak, and E_L is the peak center. Figure 9 compares, for 37.7 and 46.4 mmol/g gas loading, the resolution-broadened fits to the experimental data within the roton region $Q =$ 1.95 Å^{-1}. The data and fits clearly show that the confined liquid supports more than one mode within the roton region. For $Q = 1.95$ Å, the χ^2 values are 0.9 and 1.4 for the 37.7 and 46.4 mmol/g gas loadings, respectively. In the lower filling case, the data is fit to two broad peaks close in energy, leading to significant correlations between the two peak centers (correlation coefficient $s = 0.86$) and between the area and width of the Gaussian peak ($s = 0.90$). In the higher filling case, the two peak centers are not significantly correlated.

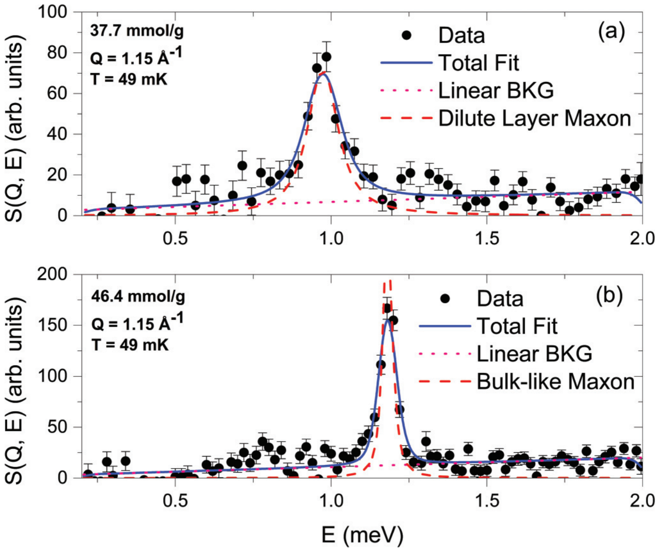

FIG. 8. (Color online) Fits to the inelastic neutron scattering data near the maxon at $Q = 1.15$ Å^{-1} for 37.7 and 46.4 mmol/g gas loadings. The solid blue curve is the total fit to the data, folding in the resolution of the neutron spectrometer. The dashed red curve is the intrinsic DHO peak corresponding to the maxon excitation. The downward shift of the maxon energy at 37.7 mmol/g pore filing is pronounced. The dotted pink line is the (multiphonon) background (BKG).

However, the oscillator strength $Z(Q)$ is strongly correlated with the FWHM Γ ($s = 0.94$). Therefore, the peak intensities and line widths should be interpreted with some caution.

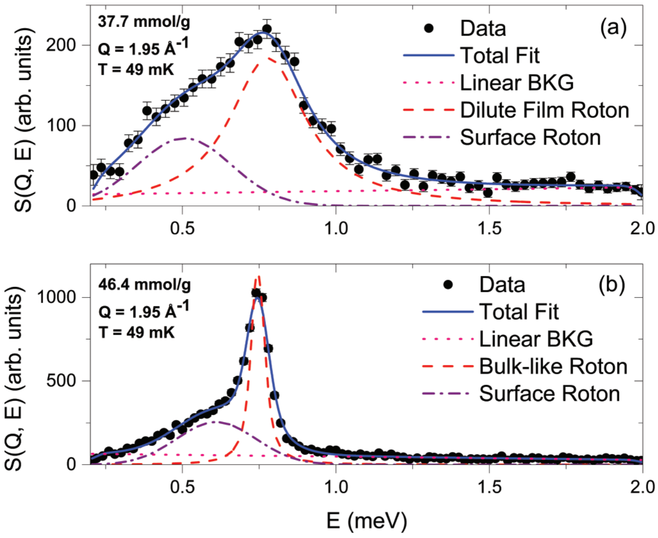

FIG. 9. (Color online) Fits to the inelastic neutron scattering data near the roton at $Q = 1.95$ Å^{-1} for 37.7 and 46.4 mmol/g gas loadings. The solid blue curve is the total fit to the data, folding in the resolution of the neutron spectrometer. In addition to a single DHO peak (dashed red line), the scattering data includes a Gaussian contribution from the surface roton (dashed dotted purple curve). Both curves shown are the intrinsic line shapes. The presence of both species of roton is immediately evident in the data. The dotted pink line is the (multiphonon) background (BKG).

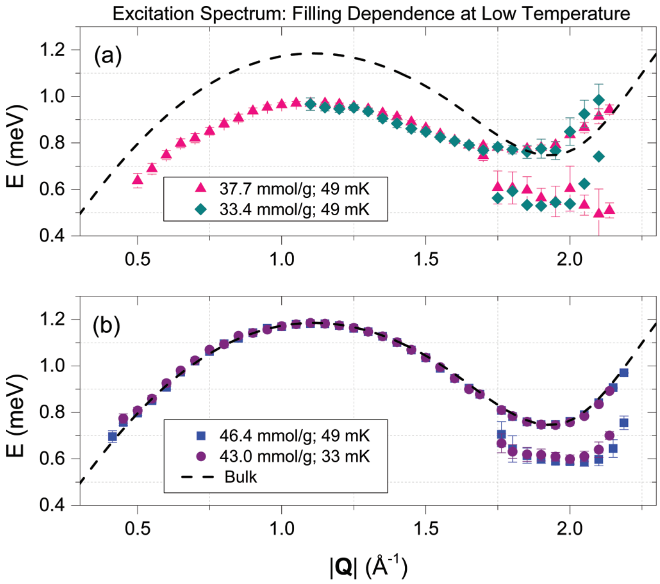

FIG. 10. (Color online) The elementary excitation spectrum of ^{4}He adsorbed within 28 Å pores. In the upper panel, the adsorbed superfluid forms a liquid film 1–2 atomic layers thick and supports a phonon-roton spectrum which is dramatically different from that of the bulk liquid. The lower panel plots the spectrum when the pores are saturated with liquid. In both regimes, an additional branch of surface rotons are observed. The error bars for the surface roton, or compressed layer mode, on the 33.4 mmol/g gas loading points have been suppressed for clarity of the figure.

The DHO peak provides an alternative model to a single Gaussian for the CLM line shape and has a clear physical motivation. Fitting the contribution to the scattering from the CLM with a DHO peak leads to essentially the same peak positions as the Gaussian. However, we found that the model fit parameters of the two DHO peaks, including the peak positions, are nearly perfectly correlated. Therefore, the Gaussian line shape model provides a more reliable determination of the CLM energy, lifetime, and spectral weight than the DHO model.

D. Excitation energies

The measured excitation energies at fillings of 33.4 and 37.7 mmol/g, where the helium forms a film less than 1 nm thick, are shown in Fig. 10(a). The observed DLM energies exhibit considerable differences from the bulk phonon-roton spectrum,[34,49,61] which is also shown in the figure. The phonon branch at low Q has a lower slope than the bulk, indicating a reduced velocity of sound, while the maxon is considerably lower in energy than the bulk value. The roton region can be fit to the Landau spectrum $E(Q) = \Delta + \hbar^2(Q - Q_R)^2/2\mu$, where Δ is the roton energy gap, Q_R is the position of the minimum, and μ is the effective mass of the roton. The properties of the dilute layer roton were determined by a least squares fit to $E(Q)$ versus Q. Compared to the bulk roton, the dilute layer roton is shifted to lower momentum, and has a higher energy and effective mass. As the filling is increased above 37.7 mmol/g, the excitation spectrum exhibits a qualitative change as shown in Fig. 10(b) for fillings of 43.0 and 46.4 mmol/g. The phonon-roton-maxon spectrum becomes nearly, but not exactly, identical to that of the bulk. The roton energy gap Δ and position Q_R of the bulklike roton is

TABLE I. Properties of the DLM, bulklike modes, and true bulk excitations are compared.

Excitation	Δ (meV)	Q_R (Å^{-1})	μ (amu)	c (m/s)
Bulk	0.742 ± 0.001	1.920 ± 0.002	0.54 ± 0.02	238
DLM	0.773 ± 0.001	1.782 ± 0.006	1.80 ± 0.08	186 ± 3
Bulklike	0.743 ± 0.001	1.924 ± 0.003	0.78 ± 0.04	228 ± 3

the same as the true bulk roton within experimental precision. However, the effective mass μ is sensitive to small differences in the curvature of the roton region, and the difference between the effective mass of the bulklike roton and the true bulk roton is a reflection of a subtle difference in curvature.

The phonon velocity c was obtained by fitting $E(Q)$ versus Q to a linear dispersion $\hbar cQ$ within the phonon region $Q \leqslant 0.7$ Å^{-1}. The phonon velocity of the thin film is reduced from the bulk speed of first sound 238 to 186 ± 3 m/s. Near full pore, the phonon velocity is increased to 228 ± 3 m/s, which is closer to the true bulk value. The values for the fit parameters are listed in Table I.

The CLM also have a parabolic dispersion in the vicinity of the roton minimum. At low pore fillings, the statistical precision of their energies is insufficient to reliably determine the properties of the CLM. When the pores are saturated with liquid, it can be seen that the roton minimum Q_{CLM} is shifted from the bulk value to higher Q, reflecting the higher density of the liquid layers they inhabit. The energy gap of the CLM depends upon the local adsorption potential of the porous host and therefore varies between different materials. The typical energies of these surface rotons is between 0.5–0.6 meV. Table II compares the properties of the compressed layer roton in FSM-16 with its values in other porous silica glasses.

E. Excitation lifetimes

On the present spectrometer, bulk phonon-roton signals would appear as resolution-limited Gaussian peaks since the intrinsic line shape is essentially a δ function. In contrast to the excitations of the bulk liquid, the DLM have a finite lifetime even at very low temperatures. Figure 8(a) illustrates the fit to the dilute layer maxon peak at $Q = 1.15$ Å^{-1}. The intrinsic FWHM of the peak is found to be 100 ± 20 μeV, about twice as broad as the instrumental resolution at that energy transfer. Figure 9(a) plots the fit to the dilute layer roton at $Q = 1.95$ Å^{-1}. The intrinsic FWHM of the dilute layer roton is found to be 300 ± 30 μeV which is about five resolution widths. Given the time-energy uncertainty principle $\delta E \delta t \geqslant \hbar/2$, the lifetimes of the dilute layer maxon and dilute layer roton are 3.3 and 1.1 ps, respectively.

TABLE II. The properties of CLM in different porous media are compared.

Matrix	Δ_{CLM} (meV)	Q_{CLM} (Å^{-1})	μ_{CLM} (amu)
FSM-16	0.597 ± 0.007	1.94 ± 0.01	0.9 ± 0.1
Aerogel (Ref. 15)	0.63 ± 0.01	1.98 ± 0.01	0.60 ± 0.04
Vycor (Ref. 14)	0.3 ± 0.2	1.87 ± 0.10	0.1 ± 0.5
Vycor (Ref. 15)	0.55 ± 0.01	1.94 ± 0.01	0.52 ± 0.04
MCM-48 (Ref. 19)	0.436 ± 0.003	2.02 ± 0.01	
Geltech (Ref. 17)	0.60		
Xerogel (Ref. 16)	~0.7		

The bulklike excitations are more sharply defined, and the peaks in the scattering data are only slightly broadened over instrumental resolution. Figure 8(b) displays the fit to the bulklike maxon, where the observed peak width is 12% broader than the instrumental resolution of 48 μeV. According to the model fit, the intrinsic line width of the bulklike maxon is 25 ± 4 μeV, corresponding to a lifetime of 13 ps. Figure 9(b) shows the bulklike roton at 46.4 mmol/g loading has an intrinsic width of 40 ± 5 μeV or an 8-ps lifetime. However, at 43.0 mmol/g, the intrinsic FWHM of the roton peak at 1.95 Å^{-1} is 76 ± 7 μeV, which is broadened 57% over the instrumental resolution.

The compressed layer roton in FSM-16 is a strongly damped excitation, as also observed in other porous media. At $Q = 1.95$ Å^{-1}, Fig. 9(a) shows that the compressed layer roton peak has an intrinsic FWHM of 400 ± 200 μeV, corresponding to a brief lifetime of 0.8 ps. At 46.4 mmol/g gas loading, shown in Fig. 9(b), the compressed layer roton remains broad, with a FWHM of 300 ± 10 μeV, enduring for 1.1 ps. In aerogel and Vycor, the compressed layer roton is reported to have a line width of 300–400 μeV.[15]

F. Peak intensities

The spectral weights of the excitations as a function of wave vector Q are shown in Fig. 11. At 37.7 mmol/g gas loading, where the adsorbed helium forms a thin film on the pore walls, the excitation spectrum consists of the modified phonon-roton spectrum, what we have called the DLM, and the surface rotons, or CLM. The intensity of the DLM, as measured by the oscillator strength $Z(Q)$, is small within the phonon region $Q < 0.7$ Å^{-1} and increases monotonically with Q through the maxon and roton regions. In contrast, the spectral weight of the compressed layer roton, as measured through the integrated peak area A, remains roughly constant with Q. The statistical error on these peak intensities is large

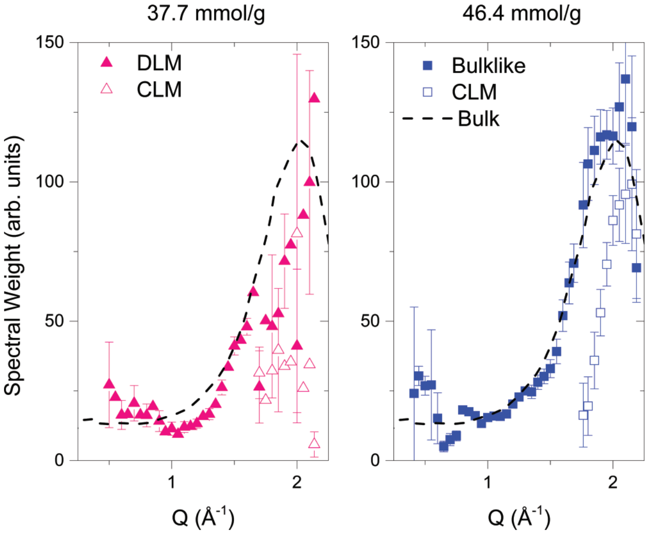

FIG. 11. (Color online) The spectral weight of the DLM, CLM, and bulklike excitations are shown versus wave vector Q.

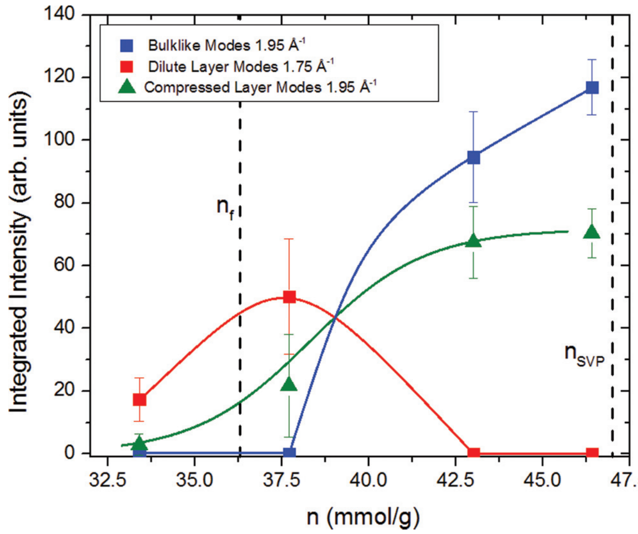

FIG. 12. (Color online) The evolution of the roton spectral weight with pore filling is shown here. The solid curves are guides to the eye.

due to the weak scattering at low pore fillings, as well as to the fact that these peaks in $S(Q,E)$ are broad and close together, as shown in Fig. 9(a). At 46.4 mmol/g gas loading, the excitation spectrum consists of phonon-roton modes at bulk energies and CLM, as in other porous media. Figure 12(b) shows that the oscillator strength $Z(Q)$ of the bulklike modes has the same Q dependence as the bulk liquid.[34] Furthermore, the CLM are not observed below $Q = 1.75$ Å^{-1}, and their intensity builds monotonically up to about 2 Å^{-1}. Measurements of $S(Q,E)$ beyond the roton region in aerogel by Azuah *et al.*[62] show that the energies and oscillator strengths $Z(Q)$ of the modes continue to show bulklike for 2 Å^{-1} $< Q <$ 3 Å^{-1}. One might therefore suspect that, for higher Q, $Z(Q)$ at 46.4 mmol/g gas loading would have the same Q dependence as the bulk liquid.

The evolution of the spectral weights of the bulklike, dilute layer, and compressed layer rotons near the respective minima with pore filling are compared in Fig. 12. The intensity of the CLM saturates as the pores are filled, which is due to the fact that they inhabit liquid layers adjacent to the interface and gain no further spectral weight after these layers are completed. The intensity of the DLM initially builds up as the thickness of the film grows, but it drops to zero as the bulklike modes appear. Further study within the crossover region would provide information about the transition in the excitation spectrum from the thin film regime to the saturated pore regime. Precisely how the peak intensities vary within this region is presently unknown.

V. DISCUSSION

A. The role of density and disorder

The dependence of the bulk spectrum upon density provides a compelling basis for a simple interpretation of the observed dispersion in FSM-16 summarized in Fig. 10. When the bulk liquid is under positive pressure or increased density, the phonon-roton modes are modified from their energies at saturated vapor pressure in the following ways: (1) the phonon velocity is increased; (2) the maxon energy is enhanced; (3) the roton minimum Q_R is shifted to higher Q; and (4) the roton energy gap Δ is decreased.[34,63] Under negative pressure or decreased density, the opposite behavior is expected on the basis of quantum Monte Carlo calculations.[35,36] Two-dimensional helium films[31–33] form a more weakly bound condensed phase than the bulk liquid, and therefore its phonon-roton spectrum shares this qualitative microscopic behavior with the liquid under negative pressure.

Our ^{4}He gas sorption measurements show continuous film growth as gas is dosed to the sample. At 33.4 and 37.7 mmol/g gas loading, there is a fluid film 1–2 atomic layers thick on top of the inert solid directly adsorbed to the pore walls. This fluid film supports a dramatically modified phonon-roton spectrum where, in comparison with the bulk liquid, the phonon velocity is decreased; the maxon energy is decreased; the roton minimum Q_R shifted to lower Q; and the roton energy gap Δ is enhanced. We have called these phonon-roton excitations DLM because their energies are consistent with those of a low-density film, one in which the typical interatomic spacing is greater than in the bulk liquid. Because long-wavelength excitations are supported, the film must have expansive and interconnected regions on the nanometer-length scale which are at low density. This provides the microscopic basis for the observations of Wada *et al.*[7,27–29] that the speed of sound is reduced at low pore fillings and the variation of the heat capacity C with T^2. This also provides a confirmation of Apaja and Krotscheck's prediction[33] that one may observe a low-density film within materials that have a uniform distribution of small pores.

The density of the adsorbed thin film can be estimated in two independent ways. First, the equation of state of liquid helium has been theoretically calculated using quantum Monte Carlo methods.[36] At the lower gas loadings studied here, the phonon velocity is observed to be 186 ± 3 m/s, which corresponds to a negative pressure of $P = -5$ bar or a density of 0.135 g/cc. Secondly, the experimentally observed dependence of the bulk roton parameters[63] upon density can be extrapolated into the negative pressure regime. This method of estimating the density of the film yields densities within the range 0.12–0.14 g/cc, consistent with independent estimates of the film density based on the theoretical equation of state. Very thin films of superfluid helium adsorbed to graphite show modest reduction in the energy of the maxon, and this reduction in energy is explained by the lower density of fluid layers on top of the inert solid ones.[9] In FSM-16, the shift in the maxon energy is more pronounced than in graphite, a reflection of lower densities realized within this material.

In addition to the DLM, we observe that the thin film also supports 2D surface rotons, which appear as an additional branch of excitations below the roton minimum. We have called these rotonlike excitations CLM because their energies are consistent with that of a dense liquid where the interatomic spacing is less than in the bulk liquid. Because rotons are short-wavelength excitations, it is likely that the film contains smaller regions or patches at higher density. One may speculate that the CLM are in some sense localized within these regions. This seems consistent with the fact that rotons have either zero or small group velocities.[20] However, the local variation in the adsorbed film density requires further explanation, and a natural source to consider is the heterogeneity of the pore walls.

Previous neutron scattering studies of liquid helium within porous silica have typically focused on porous media with irregular pore geometries and rough internal surfaces. Within such materials, the atomic-scale irregularities of the substrate increase the effective strength of the local adsorption potential.[25] The lateral mobility of adsorbate is reduced by roughness, and the rotational wave functions of adsorbed molecules are perturbed by hindering potential barriers. This is reflected in pulsed gradient NMR studies ^{3}He diffusion within porous silicas.[22–24] At low temperatures and gas loadings, where quantum-mechanical tunneling makes up the predominant motion of the adsorbed ^{3}He, the probability amplitude for an adsorbed ^{3}He atom to tunnel from one adsorption site to another depends upon the height of the potential barrier between those sites. Nuclear magnetic resonance studies have shown that, in the quantum tunneling regime, the relaxation time of ^{3}He adsorbed to FSM-16 is shorter than Vycor, a disordered spongelike glass, and MCM-41, a template silica glass morphologically similar to FSM-16.

It is therefore plausible that the overall smoothness of the FSM-16 pore walls permits the formation of a film with expansive and interconnected regions at low density; where atomic-scale disorder and roughness is present, the liquid is locally compressed due to the higher effective adsorption potential there. Therefore, the excitation spectrum consists of an extended phonon-roton spectrum corresponding to a dilute film, while the dense liquid supports a separate branch of localized, short-wavelength surface rotons. Other porous materials have generally not permitted the observation of a dilute layer roton at partial pore fillings because the roughness of the substrate is simply too great. The level of surface roughness is a possible determining cause of whether DLM will exist at low fillings and of their coexistence with CLM.

When the pores are nearly saturated with superfluid helium, a different picture of the confined liquid applies. When the solid layer is taken into account, the ^{4}He adsorption isotherm is consistent with the remaining liquid having an average density slightly greater than bulk. Bulklike liquid is packed into the core volume of the pores, compressing the liquid layer at the liquid-solid interface. The excitation spectrum therefore consists of bulklike phonon-roton modes which propagate within the core volume of the pores and CLM existing at the interface with the solid. This is the "global picture" which unifies the excitations of superfluid helium within confining geometries.[1] Compressed layer modes are typically observed within the roton region only, although they have been predicted to exist at all wave vectors.[33] One possible explanation is that the intensity of these long-wavelength CLM is simply too weak to be observed experimentally. Alternately, one may speculate that surface roughness, which is not included in those theoretical calculations, is disruptive to the formation of those longer wavelength modes.

B. Line shape broadening mechanisms

Neutron spin echo studies of bulk liquid helium[64,65] have shown that the line widths of phonon-roton peaks become vanishingly small, less than 1 μeV, at $T \ll 1$ K. On the present spectrometer, the bulk modes would appear in the experimental dynamic structure factor $S(Q,E)$ as resolution-limited peaks with a width of 56 μeV. At 37.7 mmol/g gas loading, the dilute layer roton at wave vector $Q = 1.95$ Å^{-1} is observed to have an intrinsic width of 300 ± 30 μeV. This clearly distinguishes the lifetime of the dilute layer roton from the bulk roton excitation. At 46.4 mmol/g gas loading, the bulklike roton is observed to have an intrinsic width of 40 ± 5 μeV. It is therefore interesting to inquire into the peak broadening mechanisms that distinguish the dilute layer roton and bulklike roton from each other and from the true bulk roton.

In thin films, it was suggested that the lifetimes of bulklike phonon-roton modes are limited by scattering from the boundaries of the film.[8] However, it is unlikely that this kinetic mechanism also determines the lifetime of the dilute layer roton. The root-mean-square velocity v_{rms} of a roton excitation is given by $v_{\mathrm{rms}} = \sqrt{3k_BT/\mu}$. The mean free path l is estimated to be $v_{\mathrm{rms}}\tau$, where τ is the excitation lifetime determined using intrinsic line widths. Given the effective mass μ of 1.80 amu and the lifetime τ of 1.1 ps, the mean free path l is 0.03 nm, which is smaller than the size of helium atoms. Clearly, this simple kinetic model cannot account for the strong damping of the dilute layer roton.

The relationship between the sharp phonon-roton excitation spectrum of the bulk liquid and Bose broken symmetry is a fundamental issue in the study of liquid ^{4}He.[60] Mayers[66] has argued that the δ-function phonon and roton peaks in the bulk liquid are due to long-range phase coherence in the many-particle wave function, which therefore implies the presence of a Bose condensate. One may speculate that the lifetime of the DLM may be due to the fact that 2D films cannot support a Bose condensate in the sense of off-diagonal long-range order.[3,4,67] In the absence of a Bose condensate, rotons may not be such sharply defined excitations. Because the torsional oscillator measurements of Ikegami *et al.*[28] suggest a modified Kosterlitz-Thouless phase transition at the superfluid onset, it is possible that the many-particle wave function of the film does not have requisite structure to support roton peaks in the shape of δ function. There have been attempts to directly study the topological order of thin helium films in porous media using deep inelastic neutron scattering.[68] Further theoretical work of the nature of phonons and rotons in 2D films may clarify this issue.

The phonon-roton spectrum of bulk liquid helium exhibits distinctive temperature dependence.[34,63] As the temperature is increased, the roton energy gap Δ decreases, and the intrinsic line widths Γ become increasingly broad. According to the Bardell-Pines-Zawadowski (BPZ) theory,[69] the softening of the roton mode and the duration of its lifetime at a given equilibrium temperature is due to roton-roton scattering, where the mean free path of the rotons is determined by the thermal population of excitations. The detailed calculations of the BPZ theory predict, in good agreement with inelastic neutron scattering data over a wide range of temperatures,[70,71] that the roton energy gap $\Delta(T)$ and line width $\Gamma(T)$ are given by the thermal population of rotons (to first approximation proportional to $\sqrt{T}e^{-\Delta/k_BT}$) and the $l = 0$ moment of the roton-roton interaction from roton

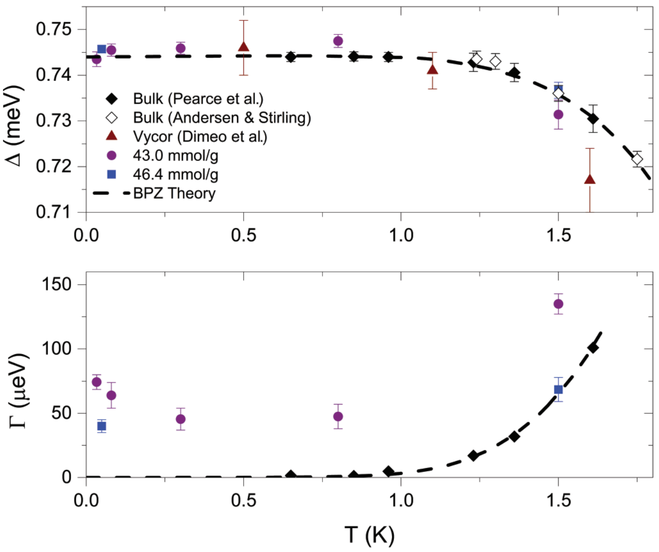

FIG. 13. (Color online) The variation of the energy gap Δ and line width Γ in the roton region at $Q = 1.925$ Å^{-1} is compared in the saturated pore regime with the bulk liquid. The energy gap Δ of the bulklike roton has the same temperature dependence as the energy gap in the true bulk liquid, and agrees, to this level of experimental precision, with the BPZ theory. In contrast to the bulk liquid, the intrinsic line widths Γ of the confined liquid appear to be finite at low temperature. However, we caution that the spectrometer resolution is 56 μeV.

liquid theory:

$$\Delta = \Delta_0 - P_\Delta(1 + R\sqrt{T})\sqrt{T}e^{-\Delta/k_B T},$$
$$\Gamma = P_\Gamma(1 + R\sqrt{T})\sqrt{T}e^{-\Delta/k_B T},$$

where Δ_0 is the roton energy gap at zero temperature, while P_Δ and P_Γ are free, phenomenological parameters usually determined by least-squares fit to neutron scattering data. The constant R accounts for cubic corrections to the roton dispersion. In Fig. 13(a), experimental values for the roton energy and lifetime are compared with the predictions of the BPZ. The agreement clearly shows that, in the bulk liquid, roton-roton scattering is the predominant mechanism responsible for the softening and damping of the roton mode.

Recent high-resolution studies (0.2 μeV) have shown small deviations from the BPZ theory, suggesting that the coupling of rotons to a thermal bath of phonons makes a contribution to the roton energy gap at very low temperatures.[72] However, these effects are too small to make a significant contribution to our dataset.

We observed that the peak energies at all Q and all gas loadings show little dependence on temperature below 1 K. However, at 1.5 K, the roton energy gap Δ is softened for the 43.0 and 46.4 mmol/g gas loadings. In Fig. 11(a), the excitation energy at $Q = 1.925$ Å^{-1} is compared with the energy gap Δ of the bulk liquid and the BPZ theory. The data is consistent with BPZ-type temperature dependence in the energy gap of the roton. Also shown is the observed temperature dependence of the bulklike roton energy gap in Vycor.[73] It seems that roton-roton scattering continues to be the predominant mechanism softening the bulklike roton in confinement.

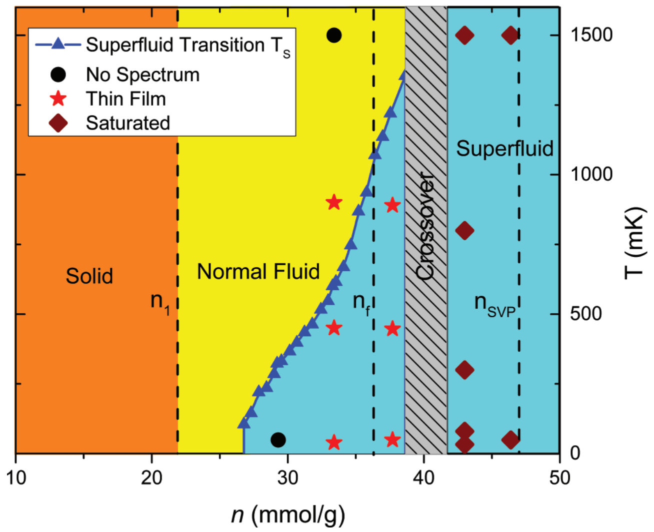

FIG. 14. (Color online) The temperature-filling phase diagram of ^{4}He confined within 28 Å pores is shown here. The blue triangles denote the superfluid onset temperature T_s determined by the torsional oscillator measurements of Ikegami *et al.* The black circles indicate conditions under which no well-defined excitations were observed. The red stars show pore fillings and temperatures in the thin film regime where the dispersion shown in Fig. 5(a) is observed. Finally, the maroon diamonds denote conditions where the dispersion shown in Fig. 5(b) is observed.

The FWHM Γ as a function of temperature is shown in Fig. 13(b). As the temperature is raised in the bulk liquid, the roton peak broadens from essentially zero width as more rotons are thermally excited. In contrast, we observe that the bulklike roton in FSM-16 has finite width at low temperatures where the density of rotons is small. Plantevin *et al.* reported that, in Geltech, bulklike phonon-roton modes have finite widths at low temperature.[17] At 1.5 K, the bulklike modes are broadened over their low-temperature widths. It is interesting to note, at this temperature, the line width at 43.0 mmol/g gas loading is considerably greater than both the predictions of the BPZ theory and the measured line width at 46.4 mmol/g gas loading.

C. Phase diagram

Figure 14 plots the filling-temperature phase diagram of ^{4}He confined in FSM-16. Below a gas loading of $n_1 = 21.9$ mmol/g, the adsorbed helium is tightly bound to the pore walls and forms an amorphous solid. This is reflected in the ^{4}He gas sorption isotherm by the vapor pressure being identically zero within experimental precision. The dynamic structure factor $S(Q,E)$ and effective vibrational density of states $G(E)$ show that this "inert" material does not support well-defined phonon excitations. The torsional oscillator measurements of the superfluid onset temperature T_S by Ikegami *et al.*[28] divide the higher gas-loading regime into a normal fluid region and a superfluid region. The superfluid onset of these films is a finite-sized Kosterlitz-Thouless phase transition. In general, our measurements of the phase diagram agree with the phase boundaries previously determined by torsional oscillator measurements, with a slight disagreement for one point close to that boundary. This may be due to the fact that different batches of FSM-16 were used in the torsional oscillator measurements and the inelastic neutron scattering experiment.

When the adsorbed helium forms a thin fluid film on the pore walls, we observe DLM, an extended phonon-roton spectrum with energies consistent with those of a low-density film. The film thickness δ and isothermal compressibility κ_T plotted in Fig. 4 indicate that, at n_f, a complete second layer has formed on top of the solid layer.[43,52] The DLM present in the film provide a microscopic basis for the thermodynamic data which shows that speed of first sound is lower than the bulk as well as the T^2 temperature dependence of the heat capacity C.

Beyond a crossover region, the excitation spectrum changes dramatically. Bulklike phonon-roton modes are observed close to n_{SVP} where the pores are completely full of superfluid helium. Their energies closely match the dispersion of the phonon-roton excitations of the bulk liquid. Aside from the presence of the CLM at low energy, the effective density of states $G(E)$ also coincides with the bulk liquid.

The behavior of the spectrum within the crossover region, and how exactly the normal-superfluid phase boundary extends to higher pore fillings, is unknown at present.

VI. CONCLUSIONS

In this paper, we reported an inelastic neutron scattering study of liquid ^{4}He confined within smooth, ordered pores only a few nanometers in diameter. The sample was carefully characterized by a combination of x-ray diffraction measurements and N_2 and ^{4}He gas sorption isotherms. The ^{4}He gas isotherms provide information about the thickness δ and 2D isothermal compressibility κ_T of the adsorbed film. The neutron scattering data distinguishes between two distinct filling regimes which support well-defined elementary excitations. At low pore fillings, when the adsorbed helium forms a superfluid film about 1–2 atomic layers thick, the excitation spectrum consists of strongly modified phonon-roton modes and an additional branch of surface rotons. In particular, the modified phonon-roton modes show a reduced phonon velocity, depression of the maxon energy, a shift of the roton minimum Q_R to lower Q, and an enhancement of the roton energy gap Δ. At high pore fillings, the excitation spectrum consists of bulklike phonon-roton modes and the separate branch of surface rotons. The qualitative difference between these two filling regimes is reflected in the effective vibrational density of states $G(E)$.

We argued that the excitation spectrum in both filling regimes can be understood in terms of the local density of the liquid. The adsorbed thin film is at low density and has larger interatomic spacing than the bulk liquid. Patches of atomic-scale surface roughness may be responsible for producing localized surface rotons. When the pores are nearly full, the liquid near the pore walls is compressed by the packing of bulklike liquid within the core volume of the pores.

Two open questions remain. First, how the excitation spectrum evolves with gas loading in the crossover from one filling regime to the other is unknown. Second, further experimental determinations of the intrinsic line widths of the phonon-roton peaks as a function of temperature would provide a more detailed picture of the peak broadening mechanisms in confinement. These are promising topics for future investigation.

ACKNOWLEDGMENTS

This research at Oak Ridge National Laboratory's Spallation Neutron Source was sponsored by the Scientific User Facilities Division, Office of Basic Energy Sciences, US Department of Energy. This report was prepared under Award 70NANB5H1163 from the National Institute of Standards and Technology, US Department of Commerce. The statements, findings, conclusions, and recommendations are those of the authors' and do not necessarily reflect the views of the National Institute of Standards and Technology or the US Department of Commerce. The authors wish to thank David Sprinkle for his invaluable expert assistance.

---

[1] E. Krotscheck and J. Navarro, eds., *Microscopic Approaches to Quantum Liquids in Confined Geometries* (World Scientific, Singapore, 2002).

[2] J. D. Reppy, J. Low Temp. Phys. **87**, 205 (1992).

[3] J. M. Kosterlitz and D. J. Thouless, J. Phys. C **6**, 1181 (1973).

[4] G. Agnolet, D. F. McQueeny, and J. D. Reppy, Phys. Rev. B **39**, 8934 (1989).

[5] H. Chu and G. A. Williams, J. Low Temp. Phys. **138**, 343 (2005).

[6] V. Kotsubo and G. A. Williams, Phys. Rev. Lett. **53**, 691 (1984).

[7] N. Wada, Y. Minato, T. Matsushita, and M. Hieda, J. Low Temp. Phys. **162**, 549 (2011).

[8] W. Thomlinson, J. A. Tarvin, and L. Passell, Phys. Rev. Lett. **44**, 266 (1980).

[9] H. J. Lauter, H. Gofrin, and P. Leiderer, J. Low Temp. Phys. **87**, 425 (1992).

[10] P. E. Sokol, M. R. Gibbs, W. G. Stirling, R. T. Azuah, and M. A. Adams, Nature **379**, 616 (1996).

[11] R. M. Dimeo, P. E. Sokol, D. W. Brown, C. R. Anderson, W. G. Stirling, M. A. Adams, S. H. Lee, C. Rutiser, and S. Komarneni, Phys. Rev. Lett. **79**, 5274 (1997).

[12] C. R. Anderson, K. H. Andersen, J. Bossy, W. G. Stirling, R. M. Dimeo, P. E. Sokol, J. C. Cook, and D. W. Brown, Phys. Rev. B **59**, 13588 (1999).

[13] H. J. Lauter, I. V. Bogoyavlenskii, A. V. Puchkov, H. Godfrin, A. Skomorokhov, J. Klier, and P. Leiderer, Appl. Phys. A **74**, 1547 (2002).

[14] R. M. Dimeo, P. E. Sokol, C. R. Anderson, W. G. Stirling, K. H. Andersen, and M. A. Adams, Phys. Rev. Lett. **81**, 5860 (1998).

[15] O. Plantevin, B. Fåk, H. R. Glyde, N. Mulders, J. Bossy, G. Coddens, and H. Schøber, Phys. Rev. B **63**, 224508 (2001).

[16] C. R. Anderson, K. H. Andersen, W. G. Stirling, P. E. Sokol, and R. M. Dimeo, Phys. Rev. B **65**, 174509 (2002).

[17] O. Plantevin, H. R. Glyde, B. Fåk, J. Bossy, F. Albergamo, N. Mulders, and H. Schøber, Phys. Rev. B **65**, 224505 (2002).

[18] F. Albergamo, J. Bossy, H. R. Glyde, and A. J. Dianoux, Phys. Rev. B **67**, 224506 (2003).

[19] J. V. Pearce, C. R. Anderson, P. E. Sokol, A. M. Toader, R. T. Azuah, and W. G. Stirling (in production).

[20] R. P. Feynman, *Statistical Mechanics: A Set of Lectures* (Addison-Wesley, Reading, Massachusetts, 1998).

[21] S. Inagaki, A. Koiwai, N. Suzuki, Y. H. Fukushima, and K. Kuroda, Bull. Chem. Soc. Jpn. **69**, 1449 (1996).

[22] C. P. Lusher, J. Nyéki, D. Shvarts, B. P. Cowan, J. Saunders, and D. E. W. Vaughan, J. Low Temp. Phys. **134**, 619 (2004).

[23] B. Yager, J. Nyéki, A. Casey, B. P. Cowan, C. P. Lusher, J. Saunders, D. Drung, and T. Schrig, J. Low Temp. Phys. **158**, 213 (2010).

[24] T. Matsushita, A. Kuze, R. Kawai, M. Heida, and N. Wada, J. Low Temp. Phys. **171**, 657 (2013).

[25] D. W. Brown, P. E. Sokol, and S. A. FitzGerald, Phys. Rev. B **59**, 13258 (1999).

[26] C. G. Sonwane, C. W. Jones, and P. J. Ludovice, J. Phys. Chem. B **109**, 23395 (2005).

[27] R. Toda, M. Hieda, T. Matsushita, N. Wada, J. Taniguchi, H. Ikegami, S. Inagaki, and Y. Fukushima, Phys. Rev. Lett. **99**, 255301 (2007).

[28] H. Ikegami, Y. Yamato, T. Okuno, J. Taniguchi, N. Wada, S. Inagaki, and Y. Fukushima, Phys. Rev. B **76**, 144503 (2007).

[29] Y. Matsushita, J. Taniguchi, R. Toda, H. Ikegami, T. Matsushita, M. Hieda, and N. Wada, J. Low Temp. Phys. **150**, 342 (2008).

[30] D. V. Anghel and M. Manninen, Phys. Rev. B **59**, 9854 (1999).

[31] B. E. Clements, H. Forbert, E. Krotscheck, H. J. Lauter, M. Saarela, and C. J. Tymczak, Phys. Rev. B **50**, 6958 (1994).

[32] R. E. Grisenti and L. Reatto, J. Low Temp. Phys. **109**, 477 (1997).

[33] V. Apaja and E. Krotscheck, Phys. Rev. Lett. **91**, 225302 (2003).

[34] A. D. B. Woods and R. A. Cowley, Rep. Prog. Phys. **36**, 1135 (1973).

[35] G. H. Bauer, D. M. Ceperley, and N. Goldenfeld, Phys. Rev. B **61**, 9055 (2000).

[36] A. R. Imre, H. J. Maris, and P. R. Williams, *Liquids Under Negative Pressure* (Kluwer Academic, Dordrecht, 2002).

[37] R. P. Feynman and M. Cohen, Phys. Rev. **102**, 1189 (1956).

[38] E. Manousakis and V. R. Pandharipande, Phys. Rev. B **30**, 5062 (1984).

[39] M. C. Gordillo and D. M. Ceperley, Phys. Rev. B **58**, 6447 (1998).

[40] D. M. Ceperley and E. L. Pollock, Phys. Rev. B **39**, 2084 (1989).

[41] A. Del Maestro, M. Boninsegni, and I. Affleck, Phys. Rev. Lett. **106**, 105303 (2011).

[42] M. Boninsegni, J. Low Temp. Phys. **159**, 441 (2010).

[43] N. Wada and M. W. Cole, J. Phys. Soc. Jpn. **77**, 111012 (2008).

[44] O. Glatter and O. Kratky, *Small-Angle X-ray Scattering* (Academic, London, 1982).

[45] B. D. Cullity, *Elements of X-ray Diffraction* (Addison-Wesley, Reading, MA, 1978).

[46] S. Lowell, J. E. Shields, M. A. Thomas, and M. Thommes, *Characterization of Porous Solids and Powders: Surface Area, Pore Size, and Density* (Kluwer Academic, Dordrecht, 2006).

[47] S. J. Gregg and K. S. W. Sing, *Adsorption, Surface Area, and Porosity* (Academic, New York, 1967).

[48] K. S. W. Sing, D. H. Everett, R. A. W. Haul, L. Moscou, R. A. Pierotti, J. Rouquérol, and T. Siemieniewska, Pure Appl. Chem. **57**, 603 (1985).

[49] S. Brunauer, P. H. Emmet, and E. Teller, J. Am. Chem. Soc. **60**, 309 (1938).

[50] E. P. Barrett, L. G. Joyner, and P. P. Halenda, J. Am. Chem. Soc. **73**, 373 (1951).

[51] C. Andreani, C. Pantalei, and R. Senesi, Phys. Rev. B **75**, 064515 (2007).

[52] G. Zimmerli, G. Mistura, and M. H. W. Chan, Phys. Rev. Lett. **68**, 60 (1992).

[53] E. Cheng and M. W. Cole, Phys. Rev. B **38**, 987 (1988).

[54] G. Zimmerli and M. H. W. Chan, Phys. Rev. B **38** 8760 (1988).

[55] G. Ehlers, A. A. Podlesnyak, J. L. Niedziela, E. B. Iverson, and P. E. Sokol, Rev. Sci. Instrum. **82**, 085108 (2011).

[56] S. W. Lovesey, *Theory of Neutron Scattering from Condensed Matter* (Clarendon Press, Oxford, 1984).

[57] A. Griffin, *Excitations in a Bose-condensed Liquid* (Cambridge University Press, Cambridge, UK, 1993).

[58] R. T. Azuah, L. R. Kneller, Y. Qiu, P. L. W. Tregenna-Piggott, C. M. Brown, J. R. D. Copley, and R. M. Dimeo, J. Res. Natl. Inst. Stand. Technol. **114**, 341 (2009).

[59] R. J. Donnelly, J. A. Donnelly, and R. N. Hills, J. Low Temp. Phys. **44**, 471 (1981).

[60] H. R. Glyde and E. C. Svensson, in *Methods of Experimental Physics, Neutron Scattering*, Part B, edited by D. L. Price and K. Sköld (Academic Press, New York, 1987).

[61] K. H. Andersen, W. G. Stirling, R. Scherm, A. Stunault, B. Fak, H. Godfrin, and A. J. Dianoux, J. Phys.: Condens. Matter **6**, 821 (1994).

[62] R. T. Azuah, H. R. Glyde, J. R. Beamish, and M. A. Adams, J. Low Temp. Phys. **117**, 113 (1999).

[63] J. S. Brooks and R. J. Donnelly, J. Phys. Chem. Ref. Data **6**, 51 (1977).

[64] F. Mezei, Phys. Rev. Lett. **44**, 1601 (1980).

[65] T. Keller, H. Habichit, R. Golub, and F. Mezei, Europhys. Lett. **67**, 773 (2004).

[66] J. Mayers, Phys. Rev. Lett. **80**, 750 (1998).

[67] A. Griffin, Can. J. Phys. **65**, 1368 (1987).

[68] S. O. Diallo, J. V. Pearce, R. T. Azuah, J. W. Taylor, and H. R. Glyde, Phys. Rev. B **78**, 024512 (2008).

[69] K. Bedell, D. Pines, and A. Zawadowski, Phys. Rev. B **29**, 102 (1984).

[70] K. H. Andersen and W. G. Stirling, J. Phys.: Condens. Matter **6**, 5805 (1994).

[71] J. V. Pearce, R. T. Azuah, W. G. Stirling, R. M. Dimeo, P. E. Sokol, and M. A. Adams, J. Low Temp. Phys. **124**, 573 (2001).

[72] B. Fak, T. Keller, M. E. Zhitomirsky, and A. L. Chernyshev, Phys. Rev. Lett. **109**, 155305 (2012).

[73] R. M. Dimeo, Ph.D. thesis, Pennsylvania State University, 1999.